energies

MDPI

Article

Fuzzy-Based Simultaneous Optimal Placement of Electric Vehicle Charging Stations, Distributed Generators, and DSTATCOM in a Distribution System

Ajit Kumar Mohanty [1], Perli Suresh Babu [1] and Surender Reddy Salkuti [2,*]

[1] Electrical Engineering Department, National Institute of Technology Warangal, Warangal 506004, India
[2] Department of Railroad and Electrical Engineering, Woosong University, Daejeon 34606, Republic of Korea
* Correspondence: surender@wsu.ac.kr

Abstract: Electric vehicles (EVs) are becoming increasingly popular due to their inexpensive maintenance, performance improvements, and zero carbon footprint. The electric vehicle's load impacts the distribution system's performance as the electric vehicle's adoption rises. As a result, the distribution system's dependability depends on the precise location of the electric vehicle charging station (EVCS). The main challenge is the deteriorating impact of the distribution system caused by the incorrect placement of the charging station. The distribution system is integrated with the charging station in conjunction with the distribution static compensator (DSTATCOM) and distributed generation (DG) to reduce the impact of the EVCS. This paper presents a fuzzy classified method for optimal sizings and placements of EVCSs, DGs, and DSTATCOMs for 69-bus radial distribution systems using the RAO-3 algorithm. The characteristic curves of Li-ion batteries were utilized for the load flow analysis to develop models for EV battery charging loads. The prime objective of the proposed method is to (1) Reduce real power loss; (2) Enhance the substation (SS) power factor (pf); (3) Enhance the distribution network's voltage profile; and (4) Allocate the optimum number of vehicles at the charging stations. The proposed fuzzified RAO-3 algorithm improves the substation pf in the distribution system. The fuzzy multi-objective function is utilized for the two stages and simultaneous placements of the EVCS, DG, and DSTATCOM. The simulation results reveal that the simultaneous placement method performs better, due to the significant reduction in real power loss, improved voltage profile, and the optimum number of EVs. Moreover, the existing system performances for increased EV and distribution system loads are presented.

Keywords: electric vehicles; distribution system; distributed generators; distribution static compensator; power factor

Citation: Mohanty, A.K.; Babu, P.S.; Salkuti, S.R. Fuzzy-Based Simultaneous Optimal Placement of Electric Vehicle Charging Stations, Distributed Generators, and DSTATCOM in a Distribution System. *Energies* **2022**, *15*, 8702. https://doi.org/10.3390/en15228702

Academic Editor: Chunhua Liu

Received: 23 October 2022
Accepted: 15 November 2022
Published: 19 November 2022

1. Introduction

Presently, EVs are preferred for road network transportation. Moreover, various government agencies and automobile industries are focusing on EVs due to their cheaper operating costs and because they have less of an impact on climatic change when compared to conventional engine vehicles [1,2]. As EVs are rapidly increasing, EVCSs are being integrated into the distribution system (DST). Due to this, power demand is increasing, leading to an increase in the load level in the distribution line and a system voltage drop. Increased power losses and voltage instability cause power security problems in the distribution system. The world's perception of distributed renewable energy has changed significantly in recent decades due to its added economic, political, and ecological benefits [3,4]. However, the improper placements of DGs make the operation of a sustainable distribution network more difficult and complex. DSTATCOMs are routinely installed by utility engineers to enhance the distribution system's voltage profile. In order to mitigate this problem, this paper includes simultaneous optimal sizing and citing of EVCSs, DGs, and DSTATCOMs in the distribution system.

1.1. Literature Review

The greater adoption of EVs may harm the performance of the distribution system. Moghaddam et al. [5] listed the impact of inappropriate coordination of EV charging, such as a rise in the peak demand of the load and an increase in power loss. Awasthi et al. [6] proposed a metaheuristic hybrid algorithm to identify the optimal positioning of EVCSs with initial investment costs and power quality variables of the city's Allahabad distribution system in India. Kongjeen et al. [7] presented different EV load models to examine the total power loss, load voltage fluctuation, and load current.

The planning model used in the publications above merely assigned the EVCS. However, introducing EVs into the system may result in higher voltage drops, power losses, and peak loads. In the research, dispersed sources of energy, particularly renewable energy, are used as planning techniques to mitigate the power losses and voltage dips caused by adding EVCS demands to the grid. If the EV load increases in the future, an updated electrical aisle is required to meet the enhanced load, which is expensive. The effective integration of an EVCS with renewable energy sources must be considered and encouraged for EV businesses to expand sustainably.

Yang et al. [8] discussed EV applications in DST along with the pros and cons of EVs integrated with DGs. Aljehane et al. [9] developed a model with real-time energy management, where EVCSs and DGs were optimally allocated in the distribution system using black widow optimization (BWO). Ajit et al. [10] proposed a method with a GWO algorithm to integrate EVs with DGs in a distributed system. Roudbari et al. [11] suggested a resilience-oriented operation to improve the distribution network's resiliency and economic benefits. In the recommended strategy, weather-based outages are modeled to reschedule energy resources and EV management. Piazza et al. [12] proposed a technique for defining and designing electric services for a local electricity community that obtained its energy from a microgrid that used renewable energy sources and storage devices (by using mixed-integer non-linear programming (MINLP)) . Palmiotto et al. [13] assessed the possibility of load leveling and cost minimization for a district of residential users in the presence of an aggregator while considering a realistic PV array and EV diffusion with the help of Quadprog and Linprog optimization tools (QLT). Dekaraja et al. [14] used the artificial flora algorithm (AFA) to construct a model for the optimum positioning of EV and DG. Ahmad et al. [15] provided a comprehensive model for effectively positioning solar-powered charging stations in a distribution system with an enhanced voltage profile, minimal power loss, and lower costs, with the help of the improved chicken swarm optimization (CSO). However, in this work, the substation power factor was ignored. Liu et al. [16] suggested a bi-level optimal allocating framework for DGs and EVCSs that considered the EV charging load's stochasticity, fluctuation, and output power, as well as the traditional load. Dharavat et al. [17] suggested placing numerous DGs alongside EVs while considering appropriate scheduling strategies to reduce the power loss and significantly enhance the voltage level. Biswas et al. [18] discussed the advantages of metaheuristic methods for determining the size and location of DG and shunted the capacitor in the DST to reduce the real power loss (RPL) and voltage deviations (VDs), using a multi-objective evolutionary algorithm based on decomposition (MEA/D). Bilal et al. [19] reviewed the optimal placements of fast charging stations with capacitors, which reduced power loss and enhanced the voltage profile of the DST. Gampa et al. [20] proposed a two-stage methodology using the grasshopper optimization algorithm (GOA) for optimal placement of EVCSs, DGs, and shunt capacitors. In the first stage, the DG and shunt capacitor were optimally located. Later, in the second stage, the EV was placed, although the SS pf was not considered at this stage. The above-mentioned literature [8–20] did not consider SS pf.

DGs, which include solar panels, fuel cells, and microturbines, are electrical sources of energy that generate electricity at the unity power factor (as discussed in the literature previously mentioned). DSTATCOM is employed in the distribution system to compensate for reactive power requirements. Sirjani et al. [21] comprehensively analyzed several research projects on the optimal sizings and positionings of DSTATCOM in the distribution

system. It was shown that the goals of the D-STATCOM allocation problem could include lowering power losses, minimizing voltage changes, strengthening voltage stabilities, and raising reliability metrics. Jazebi et al. [22] minimized active power losses and bus voltage fluctuations by employing a differential evaluation technique for DSTATCOM's optimum placement in the radial distribution system. DG was incorporated with DSTATCOM in the DST to further reduce active power loss [23–25]. The active power loss and voltage variation reported by Pratap et al. [26] were decreased by the simultaneous integration of DSTATCOM and DG during EVCS-loading using the African vulture optimization algorithm (AVO).

With the help of the metaheuristic technique, various optimization problems can be solved. The literature now has a large number of metaheuristic algorithms. Safari et al. [27] implemented a PSO algorithm to allocate EVs in the distribution system. Singh et al. [28] presented a grey wolf optimizer (GWO) algorithm to reduce the smart grid's power loss when EVs are used. Ponnam et al. [29] implemented the TLBO algorithm to position EVCS optimally in the distribution system. The JAYA algorithm was used to implement optimal charging station allocation in the publication [30]. To obtain a near-global optimum, they must change the parameters. Metaheuristic optimization techniques require significant and time-consuming parameter adjustments to tackle particular optimization problems. Therefore, to address the presented problem in this study, this work proposes a reliable optimization method called the RAO algorithm [31]. Investigations were made into how EV battery charging affects the effectiveness of the DST [32–34].

1.2. Contributions

Most of the literature studies surveyed only discuss the optimal allocation of EVCSs in the distribution system, which deteriorate the voltage profile and pf. As stated earlier, the DG [8–17] and shunt capacitor [18–20] are integrated into the system to mitigate this effect. However, the research on allocating DSTATCOM in DST, along with EVCS and DG into the substation power factor is still very scant [26]. Conventional multi-objective methods for optimal siting of EVCS, DG, and DSTATCOM do not consider the substation pf. As indicated in Table 1, few research studies have considered the substation power factor components of the EVCS allotment challenge with DSTATCOM and DG. Therefore, with the help of fuzzy [35,36] multi-objectives, SS pf can attain desired values. Hence, in this paper, simultaneous EVCS, DG, and DSTATCOM were allocated in the electrical distribution network, with a fuzzy multi-objective approach using the RAO-3 algorithm for better performance in the distribution network, such as minimizing active power loss, improving the voltage profile, and maintaining SS pf at the desired value. Results from various traditional algorithms, including PSO, TLBO, GWO, and JAYA, are compared to those from the suggested technique. Figure 1 depicts the proposed framework for the positioning and sizing of EVCS, DG, and DSTATCOM.

Table 1. An overview of the research gap analysis and the authors' contributions.

Ref.	EVCS	DG	DSTATCOM	Optimization Strategies	RPL	VD	SS pf	NEV
[9]	✓			BWO	✓	✓		
[10]	✓	✓		GWO	✓	✓		
[12]	✓	✓		MINLP	✓			✓
[13]	✓	✓		QLT	✓	✓		
[14]	✓	✓		AFA		✓		
[15]	✓	✓		CSO	✓	✓		
[18]	✓	✓		MEA/D	✓	✓		
[19]	✓			GWO-PSO	✓	✓		
[20]	✓	✓		GOA	✓	✓		✓
[26]	✓	✓	✓	AVO	✓	✓		✓
In this work	✓	✓	✓	RAO-3	✓	✓	✓	✓

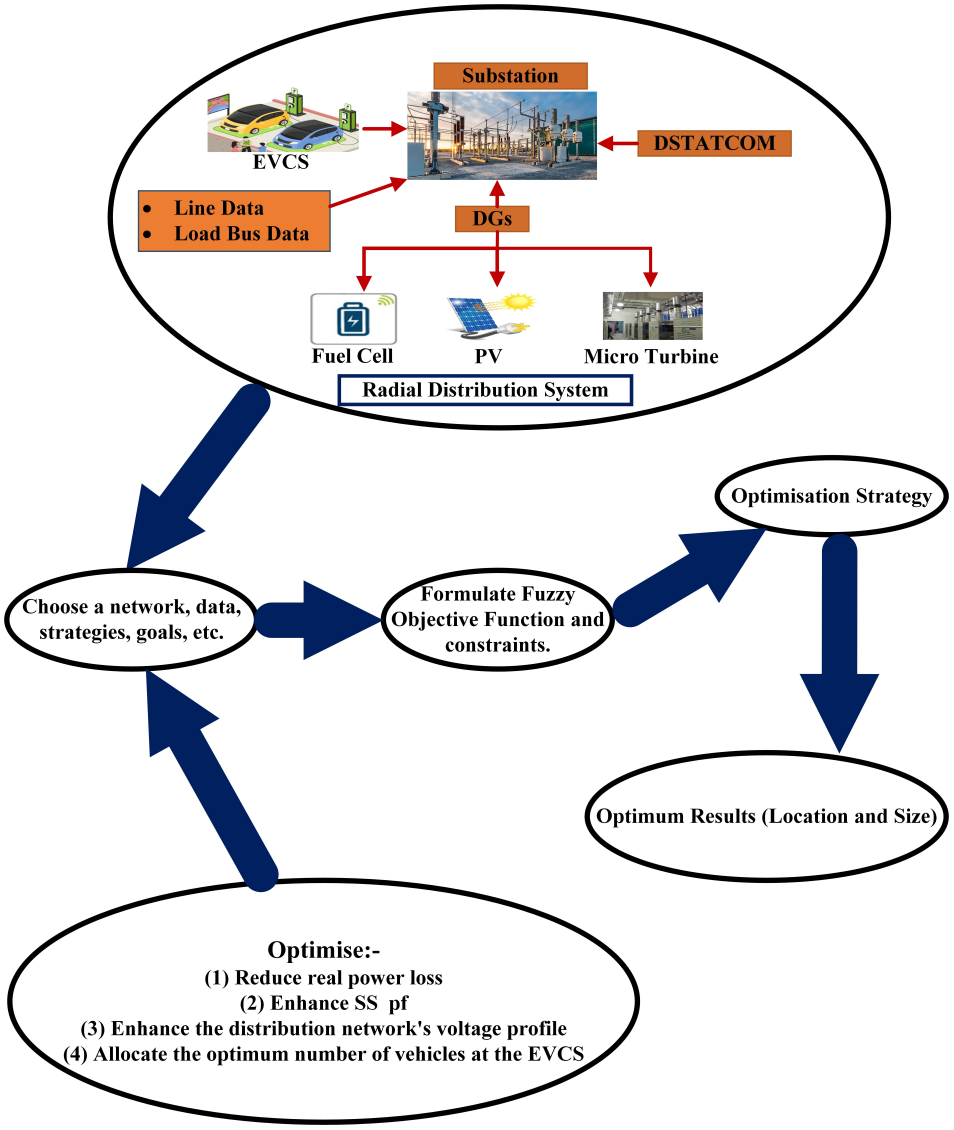

Figure 1. Synergistic planning framework of EVCS, DG, and DSTATCOM in the distribution system.

The main contributions of this study that stand out when compared to the literature are as follows:

1. The first stage involves choosing the optimum size and position for DG and DSTATCOM in the distribution system to maintain SS pf to the desired value achieved. Furthermore, in the second stage, the EVCS is optimally sized and located with the optimal number of EVs.
2. Simultaneous optimal sizing and siting of the EVCS, DSTATCOM, and DG in the distribution system to maintain SS pf to the desired value with the optimal number of EVs.
3. The optimal siting of EVCS, DG, DSTATCOM, and the optimal number of EVs to fulfill the current and future expanded EV population load.
4. In order to examine the impact of EV charging on the DST performance, load models for charging batteries were built using the load flow analysis.

The rest of the paper is structured as follows: Section 2 explains the fuzzy multi-objective problem formulation and its restrictions. In Section 3, from the battery charging characteristics, the charging load models for EV batteries were developed for the load flow analysis. Section 4 introduces the suggested fuzzy multi-objective RAO-3 method. Section 5 presents the results and analyses, and Section 6 presents the conclusions.

2. Problem Formulation

This section presents fuzzy multi-objective functions for the optimal placements of DG, DSTATCOM, and EVCS in various scenarios to improve the DST performance. This section presents the multi-objective function that focuses on reducing real power loss, enhancing the voltage profile of DST, enhancing the substation's power factor, and the optimum number of electric vehicles at the EVCS.

The fuzzy domain membership function is presented for each objective. The membership function indicates the level of goal satisfaction. In the crisp domain, the membership function values are either zero or unity, whereas, in the fuzzy domain, they range from zero to unity. Consequently, the fuzzy set theory advances the classic style theory [35]. The membership function is a strictly monotonically declining continuous function with lower and upper bound values for the various goals described below. The trapezoidal memberships are used to obtain the desired multi-objective values, such as reduced power loss and improved voltage limitations [36]. The triangular function is used for additional objectives needed to mollify constraints, such as the SS power factor and DG penetration limit [36].

2.1. Fuzzification of Real Power Loss of the DST

The real power losses of the distribution system is shown below:

$$RPL = \sum_{j=1}^{nb-1} Pl_j \tag{1}$$

$$Pl_j = \frac{r_j \times \left\{P_{j+1}^2 + Q_{j+1}^2\right\}}{\left|v_{j+1}\right|^2} \tag{2}$$

Pl_j is the assumed test distribution network's branch real power loss, where P_{j+1} is the active power load and Q_{j+1} is the reactive power load injected at the load $(j+1)$ node. In the distribution network, resistance at the jth node is r_j and the voltage at the $(j+1)$th node is v_{j+1}. The real power loss index $(RPLX)$ can be calculated as:

$$RPLX = \frac{RPL_{DGSC}}{RPL_{Base}} \tag{3}$$

RPL_{DGSC} is the active power loss with DG and DSTATCOM. The active power loss in the base situation is represented by RPL_{Base}. The fuzzified real power loss index $(\in {}^{RPLX})$ [20] is shown in Figure 2. $RPLX^{max}$ is considered unity. Based on utility necessity, $RPLX^{min}$ was selected, such that the active power loss was reduced to the desired value. The mathematical expression for the fuzzy set $\in {}^{RPLX}$ is explained in Equation (4).

$$\in {}^{RPLX} = \begin{cases} 1 & \text{for } RPLX \le RPLX^{min} \\ \frac{RPLX^{max} - RPLX}{RPLX^{max} - RPLX^{min}} & \text{for } RPLX^{max} \le RPLX \le RPLX^{min} \\ 0 & \text{for } RPLX > RPLX^{max} \end{cases} \tag{4}$$

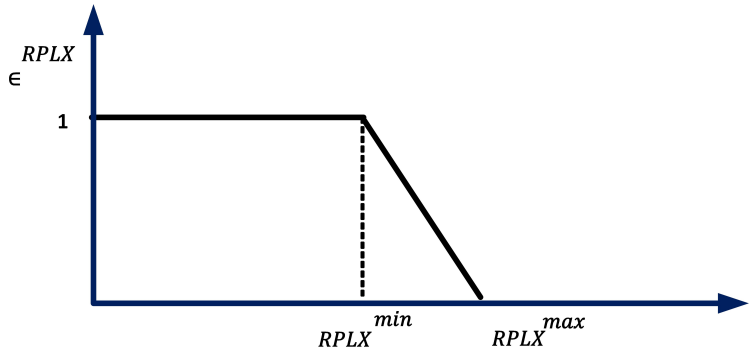

Figure 2. Reduction of real power loss.

2.2. Fuzzification of Voltage Nodes of the Distribution Network

The fuzzy membership function of voltage $(\in^{v_j})$ [20] of each node j in the distribution network is explained in Figure 3; mathematically, it can be explained in Equation (5): $v_{l1} = 0.94$, $v_{min} = 0.95$, $v_{max} = 1.05$ and $v_{l2} = 1.06$ are assumed. In this work, the fuzzy voltage performance $(\in^{v})$ is the minimum value of fuzzy membership of the voltage of each node of the distribution network considered. It can be defined as $\in^{v} = \min(\in^{v_j})$.

$$\in^{v_j} = \begin{cases} 0 & \text{for } v_j \le v_{l1} \\ \frac{v_j - v_{l1}}{v_{min} - v_{l1}} & \text{for } v_{l1} < v_j < v_{min} \\ 1 & \text{for } v_{min} \le v_j \le v_{max} \\ \frac{v_j - v_{max}}{v_{l2} - v_{max}} & \text{for } v_{max} < v_j < v_{l2} \\ 0 & \text{for } v_j > v_{l2} \end{cases} \tag{5}$$

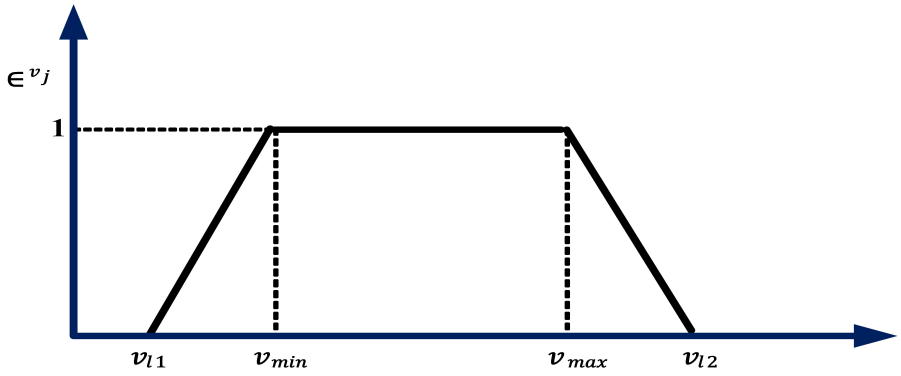

Figure 3. Bus voltage.

2.3. Fuzzification of SS Power Factor

The DG must operate at a lagged pf of 0.95 to increase the SS power factor (pf). It is possible to determine the SS power factor:

$$pf = \cos\left(\frac{S_{kW}^{SN}}{S_{kVA}^{SN}}\right) \tag{6}$$

$$S_{kW}^{SS} = \sum_{j=1}^{nb} P_j^{load} + Pl - \sum_{k=1}^{ndg} P_k^{DG} \tag{7}$$

$$S_{kVAr}^{SS} = \sum_{j=1}^{nb} Q_j^{load} + Ql - \sum_{m=1}^{nsc} Q_m^{SC} - \sum_{k=1}^{ndg} P_k^{DG} \times \varnothing_{dg} \tag{8}$$

$$S_{kVA}^{SS} = \sqrt{S_{kW}^{SS\ 2} + S_{kVAr}^{SS\ 2}} \tag{9}$$

P^{DG} is the capacity of DG. ndg stands for the number of DGs installed in the DST. The active power load connected to the jth bus is P_j^{load}, and the total number of buses in the DST is nb. When DG, DSTATCOM, or EV charging stations are deployed, The distribution network's active power loss is termed Pl. The reactive power load linked to the jth bus is Q_j^{load}, the DSTATCOM rating is Q_m^{SC}, and the total number of DSTATCOMs in the DST is nsc. When DG or DSTATCOM are implemented, the distribution network's reactive power loss is Ql.

The triangular fuzzy membership function [20] for the SS power factor $(\in^{pf})$ is shown in Figure 4 and the mathematical expression is shown in Equation (10).

$$\in^{pf} = \begin{cases} 0 & \text{for } pf \le pf_{min} \\ \frac{pf - pf_{min}}{pf_s - pf_{min}} & \text{for } pf_{min} \le pf \le pf_s \\ \frac{pf_{max} - pf}{pf_{max} - pf_s} & \text{for } pf_s \le pf \le pf_{max} \\ 0 & \text{for } pf \le pf_{max} \end{cases} \tag{10}$$

In the preceding equations, pf_{min} =0.85, pf_s =0.95, and pf_{max} = 1.0 are used. The desired power factor level is denoted as pf_s.

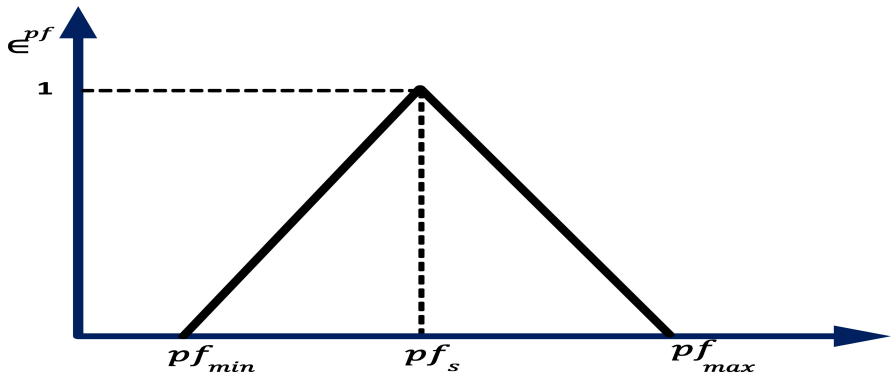

Figure 4. SS power factor.

2.4. Fuzzification of DG Penetration

Penetration of the DG index in the distribution network can be defined as the ratio of the number of DGs connected to the total real power load in the DST.

$$DGPI = \frac{\sum_{k=1}^{ndg} P^{dg}}{\sum_{j=1}^{nb} P^{load}} \tag{11}$$

Figure 5 shows the triangular fuzzification of the DG penetration $(\in^{DGPI})$ [20] limit; the mathematical expression is shown in the following Equation (12). $DGPI_{min} = 0.4$, $DGPI_s = 0.5$, $DGPI_{max} = 0.6$, respectively. $DGPI_s$ are the desired penetration levels in the distribution network. In this work, penetration is considered at 50%.

$$\in^{DGPI} = \begin{cases} 0 & \text{for } DGPI \le DGPI_{min} \\ \frac{DGPI - DGPI_{min}}{DGPI_s - DGPI_{min}} & \text{for } DGPI_{min} \le DGPI \le DGPI_s \\ \frac{DGPI_{max} - DGPI}{DGPI_{max} - DGPI_s} & \text{for } DGPI_s \le DGPI \le DGPI_{max} \\ 0 & \text{for } DGPI \le DGPI_{max} \end{cases} \tag{12}$$

2.5. Fuzzification of the EV Power Loss Index

With the EV index, the real power loss can be calculated as follows:

$$EVPI = \frac{EVPI^{EVLD}}{EVPI^{LD}} \tag{13}$$

$EVPI^{EVLD}$ is the active power loss with EV and other load losses. $EVPI^{LD}$ is the load loss. Here, the load can be DG, DSTATCOM, or any commercial load.

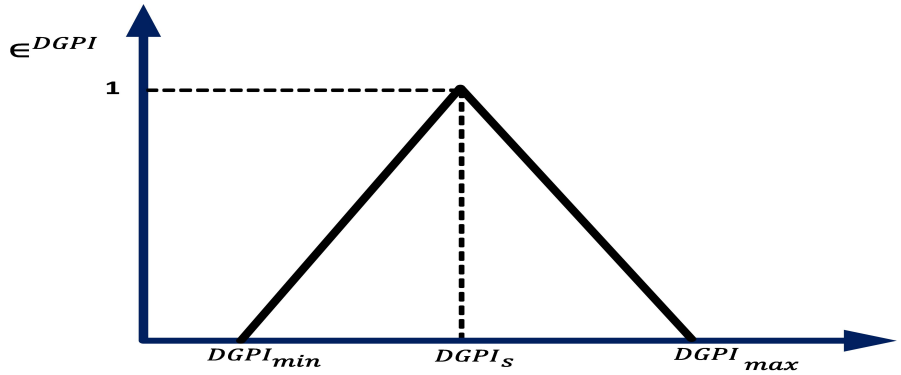

Figure 5. DG penetration.

The membership fuzzification of the EV power loss index ($\in^{EVPI}$) [20] is shown in Figure 6; the mathematical expression is shown in Equation (14).

$$\in^{EVPI} = \begin{cases} 0 & \text{for } EVPI \leq EVPI_{min} \\ \frac{EVPI - EVPI_{min}}{EVPI_s - EVPI_{min}} & \text{for } EVPI_{min} \leq EVPI \leq EVPI_s \\ \frac{EVPI_{max} - EVPI}{EVPI_{max} - EVPI_s} & \text{for } EVPI_s \leq EVPI \leq EVPI_{max} \\ 0 & \text{for } EVPI \leq EVPI_{max} \end{cases} \tag{14}$$

$EVPI_{min} = 1$, $EVPI_s = 1.5$, $EVPI_{max} = 2$ respectively. $EVPI$ is always greater than 1 because power loss increases with the addition of the EV load in the distribution network.

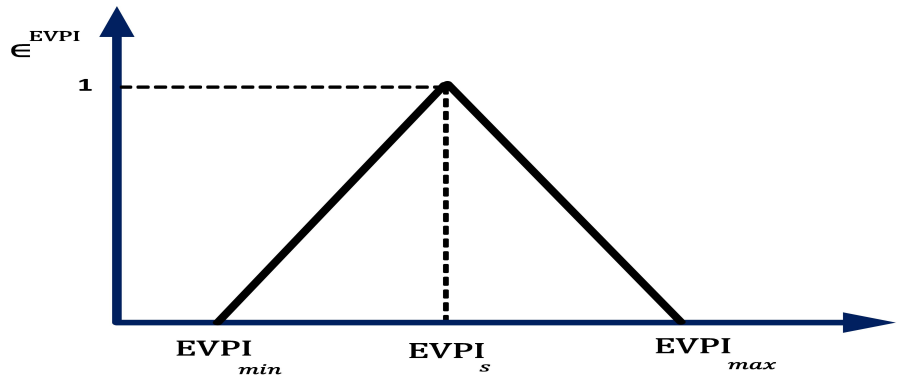

Figure 6. EV real power index.

2.6. Multi-Objective Fuzzy Function for Optimal Sizing and Location of EVCS, DG, and DSTATCOM

1. Multi-objective fuzzy functions for simultaneous optimum allocation of EVCS, DSTATCOM, and DG are shown in the following equation:

$$F_{zs} = \frac{1}{\in^{RPLX} + \in^{pf} + \in^{v} + \in^{DGPI} + \in^{EVPI}} \tag{15}$$

2. In the scenario where only DG and DSTATCOM are required to place optimally in the DST, then the following equation depicts multi-objective fuzzy functions for the DG and DSTATCOM optimum sites and sizings:

$$F_{zdc} = \frac{1}{\in^{RPLX} + \in^{pf} + \in^{v} + \in^{DGPI}} \tag{16}$$

This multi-objective function is used; EVCS is not included. Only DG and DSTATCOM are required to place optimally in the DST.

3. The following equation depicts the fuzzy objective functions for the optimum location and sizing of EVCS:

$$F_{ze} = \frac{1}{(\in^{EVPI})} \tag{17}$$

The multi-objective fuzzy functions, explained in Equations (15)–(17), are minimized by using the RAO-3 algorithm subjected to different constraints. In this work, penetration of DG in the distribution network is considered to be 50 % of the total active power load; the reactive power injection is 50 % of the total reactive power.

$$0 < P_k^{DG} \leq P_{max}^{DG} \; where \; k = 1,\ 2,\ 3 \tag{18}$$

$$0 < Q_m^{sc} \leq Q_{max}^{sc} \; where \; k = 1,\ 2,\ 3 \tag{19}$$

P_k^{DG} and Q_m^{sc} are the DG power and DSTATCOM reactive power injection at the nodes in the distribution network at optimal locations.

3. Modeling Battery Charging Load for EV

In this work, it is anticipated that EVs will be recharged from completely depleted states. Figure 7 can be used to produce the equation for the load flow analysis using the models for the battery charging loads [32]. The charging of a battery is shown in Equation (20) for both transient and steady state conditions. As a result, the exponential equations below can be used to estimate the battery power charging parameters.

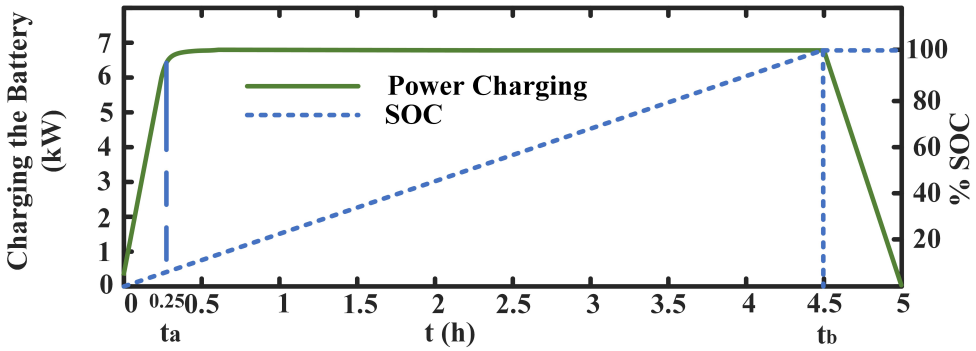

Figure 7. Li-ion battery charging characteristics.

$$P_{bEV}(t) = \begin{cases} P_{bEV}^{max}(1 - e^{\left(\frac{-\gamma \times t}{t_b}\right)}) & 0 \leq t \leq t_b \\ P_{bEV}^{max}\left(\frac{t_{max} - t}{t_{max} - t_b}\right) & t_b \leq t \leq t_{max} \\ 0 & t > t_{max} \end{cases} \tag{20}$$

$P_{bEV}(t)$ represents the instantaneous EV battery charging load. The maximum battery charging load for the substation is P_{bEV}^{max}.

$$\delta P_{bEV}^{max} = P_{bEV}^{max}\left(1 - e^{\left(\frac{-\gamma \times t_a}{t_b}\right)}\right) \tag{21}$$

$$\gamma = -\left(\frac{t_a}{t_b}\right) ln(1-\delta) \tag{22}$$

$t_a = 0.25\,h$, $t_b = 4.5\,h$, and $t_{max} = 5\,h$ are in the preceding Equations (16) and (21), respectively, taken from Figure 7. γ and δ are EV battery characteristic constants. Equation (22) (derived from Equation (21)) can be used to find the value of γ. The EV battery's characteristic constants are alpha and beta. The fraction of maximum charging load, expressed as 0.95, accounts for 95% of P_{bEV}^{max} at time t_a.

Equation (23) can be utilized to establish the power charging equation when the batteries are charged from a zero-charge scenario P_{bEV}^{0}.

$$P_{bEV}(t) = P_{bEV}^{max}\left(1 - e^{\left(\frac{-\gamma \times t}{t_{cg}}\right)}\right) + P_{bEV}^{0}\left(e^{\left(\frac{-\gamma \times t}{t_{cg}}\right)}\right) 0 < t < t_{cg} \tag{23}$$

The t_cg is the time it takes to charge a battery from its starting charge position fully. The following equation can be used to describe the state of the power-charging battery.

$$SOC(t+1) = SOC(t) + P_{bEV}(t) \times \Delta(t) \tag{24}$$

Once reaching 100 % SOC, the batteries should be unplugged from the power supply to minimize battery damage caused by overcharging.

4. Summary of RAO-3

The optimization algorithm Rao was recently created [31]. Rao-1, Rao-2, and Rao-3 are the three proposed Rao algorithms. This study chose it as a population-based approach because it is straightforward to employ in optimized applications. It also has fewer control factors because there is no metaphorical explanation. Once the halt condition is reached, only the swarm size needs to be changed. Compared to other algorithms, the RAO algorithm performs better statistically because it can ensure exploration performance while yielding superior exploitation, keeping an excellent balance between exploration and exploitation.

The three RAO algorithms follow similar processes. However, as seen in the following steps and shown in Figure 8, only the movement equation is different.

1. Initialize the system data and load profile.
2. Initialize the population (algorithm parameter), iteration, and set the maximum iteration.
3. Randomly initialize the sizings and locations of EVCS, DG, and DSTATCOM.
4. The objective function's indicated fitness function is put to the test.
5. Identify the best and worst solutions proposed by the population.
6. The revised solution is updated for all populations under the selected RAO algorithm as follows:

- RAO-1:

$$z'_{m,p,i} = z_{m,p,i} + rand_{1,m.i} \times (z_{m,b,i} - z_{m,w,i}) \tag{25}$$

- RAO-2:

$$\begin{aligned} z'_{m,p,i} &= z_{m,p,i} + rand_{1,m.i} \times (z_{m,b,i} - z_{m,w,i}) \\ &+ rand_{2,m.i} \times (|\, z_{m,p,i} \; or \; z_{m,d,i} \,| - |\, z_{m,d,i} \; or \; z_{m,p,i} \,|) \end{aligned} \tag{26}$$

- RAO-3:

$$\begin{aligned} z'_{m,p,i} &= z_{m,p,i} + rand_{1,m.i} \times (z_{m,b,i} - |\, z_{m,w,i} \,|) \\ &+ rand_{2,m.i} \times (|\, z_{m,p,i} \; or \; z_{m,d,i} \,| - (z_{m,d,i} \; or \; z_{m,p,i})) \end{aligned} \tag{27}$$

$z_{m,p,i}$ is the mth variable's value for the pth candidate in the ith iteration. The best solution is denoted by $z_{m,b,i}$, whereas the worst solution is denoted by $z_{m,w,i}$. The Rao

algorithm can guarantee exploration performance while producing superior exploitation, resulting in an excellent balance between exploitation and exploration, representing the method's higher statistical performance when compared to other algorithms.

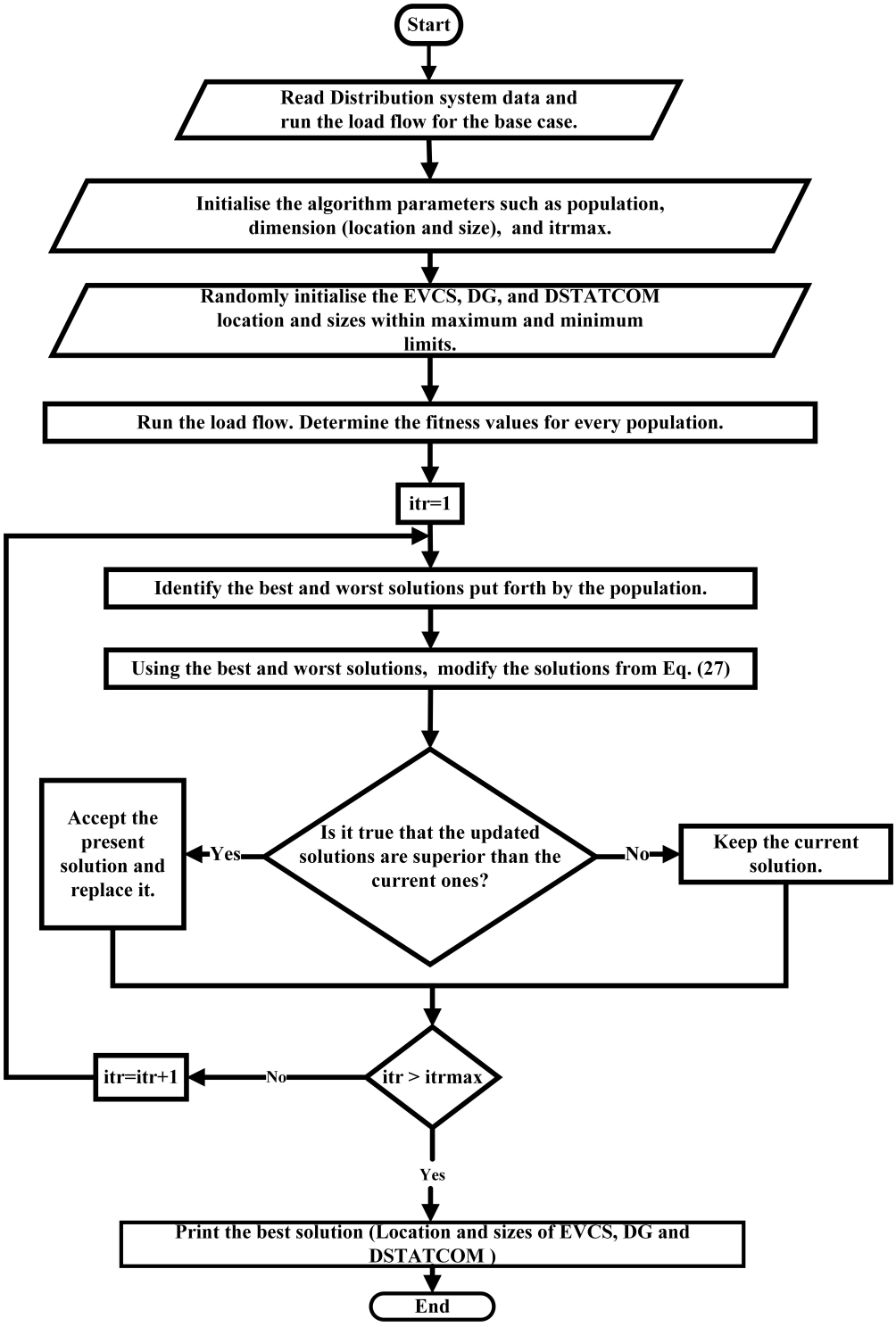

Figure 8. RAO-3 algorithm implementation flow chart.

5. Results and Discussion

A 69-bus radial distribution system is considered for the present analysis. The system's base values are 100 MVA and 12.66 kV. The backward–forward sweep method has been used for load flow studies. The proposed problem's simulation was carried out via MATLAB

2017a software installed on a computer with a processor Intel core i5 8th Gen, 8 GB RAM. Initially, i.e., at the base case from the load flow, the following data were obtained: the total real power load was 3082.19 kW, the reactive power load was 2796.77 kVAr, the minimum voltage was 0.9092 p.u., and the overall real power loss was 225 kW. The algorithm made the following assumptions: itrmax = 100 and population = 100.

The optimal positions and sizings of DG and DSTATCOM units were addressed in this work in the distribution system, which included three bus nodes of DG units and three bus nodes of DSTATCOM units. Moreover, for optimal planning of the EV charging station, five bus nodes were assumed, which is approximately 13% of the assumed distribution system bus nodes. In each charging station, a maximum of 50 EVs can be charged. The characteristic charging curve is shown in Figure 7. Figure 7 shows that the Li-ion battery's maximum constant charge charging load is 6.5 kW.

5.1. Scenarios

Two different scenarios were considered in the given DST for optimal sizings and locations of EVCS, DSTATCOM, and DG.

- Scenario 1: In this first stage, DSTATCOM and DG are integrated with the distribution network; in the second stage, EV charging stations are connected.
- Scenario 2: In the simultaneous EV charging station, DG and DSTATCOM are connected.

5.1.1. Scenario 1

In the first stage, optimum citing and sizing of DG and DSTATCOM are done, with the help of a fuzzy multi-objective function, as shown in Equation (16). This fuzzy multi-objective used in Equation (16) is considered to maintain the substation power factor desired value, improve the voltage profile, and reduce the distribution system's active power losses. Optimum allocations of DG and DSTATCOM are done with the RAO-3 algorithm's help, as shown in Tables 2 and 3. From this work, it can be seen that in the proposed method, each bus voltage moves closer to unity and the distribution system's performance is enhanced. The fuzzy RAO-3 method is compared with a two-stage methodology [20], fuzzy TLBO, fuzzy GWO, and fuzzy PSO. The performance of the distributed system, voltage profile, and convergence of fitness is better with RAO-3, as depicted in Table 4 and Figures 9 and 10.

Table 2. DG optimum location and sizing.

Fuzzy PSO		**Fuzzy GWO**		**Fuzzy TLBO**		**Fuzzy JAYA**		**Fuzzy RAO-3**	
DG Node location	DG Sizing (kW)	DG Node location	DG Sizing (kW)	DG Node location	DG Sizing (kW)	DG Node location	DG Sizing (kW)	DG Node location	DG Sizing (kW)
13	481.9379	61	887.9736	61	900.0000	61	900.0000	13	561.1438
61	737.8022	13	335.7383	23	499.5148	11	626.7025	21	643.5554
20	680.9627	23	677.1779	10	501.1851	24	373.9975	61	696.0012

Table 3. DSTATCOM optimum location and sizing.

Fuzzy PSO		**Fuzzy GWO**		**Fuzzy TLBO**		**Fuzzy JAYA**		**Fuzzy RAO-3**	
Node location	Sizing (kVAr)	Node location	Sizing (kVAr)	Node location	Sizing (kVAr)	Node location	Sizing (kVAr)	Node location	Sizing (kVAr)
64	573.4461	21	484.6605	65	654.9968	23	432.3735	22	483.9325
12	383.6421	64	549.4658	24	510.2932	69	422.2525	69	432.9390
21	495.0255	69	417.6416	12	284.7286	62	596.9364	64	538.5364

The EVCS is installed after the integration of the DG and DSTATCOM in the DST, which is the second stage. In this work, five optimum locations are preferred for locating the charging station. In each charging station, a maximum of 50 EVs are assumed. A fuzzy multi-objective was used for achieving this optimal location, as shown in Equation (17).

The optimum number of EVs and optimum locations of EVCSs are shown in Table 5. The final distribution of the active power loss and minimum voltage with DG, DSTATCOM, and EV are shown in Table 6. The single-line diagram of the 69-bus radial distribution system with EVCS, DG, and DSTATCOM of scenario 1 is shown in Figure 11.

Table 4. Performance comparison of the 69-bus system.

Scenario 1	Base Case	Two-Stage Methodology [20]	Fuzzy PSO	Fuzzy GWO	Fuzzy TLBO	Fuzzy JAYA	Fuzzy RAO-3
SS Active power (kW)	4027.19	1920.93	1921.6	1920.9	1920.8	1920.7	1920.4
SS Reactive power (kVAr)	2796.77	631.22	633.2409	631.2786	631.1990	631.0172	630.2859
SS pf	0.8214	0.95 lag	0.95 lag	0.95 lag	0.95 lag	0.95 lag	0.95 lag
DG Penetration	-	1900.11	1900.7	1900.7	1900.6997	1900.7	1900.7
RPL (kW)	224.56	27.34	28.9222	27.12	26.9835	26.7348	22.9920
Voltage minimum (p.u.)	0.902	0.9461	0.9717	0.9718	0.9728	0.9795	0.9811

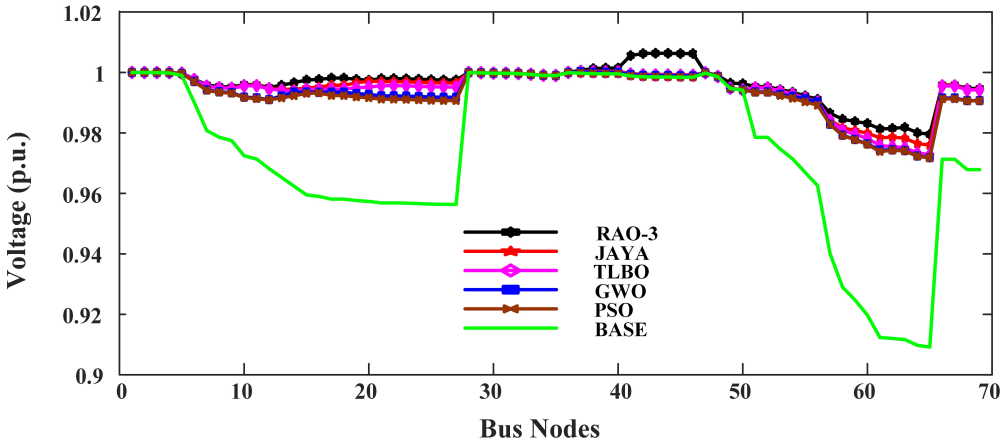

Figure 9. Voltage Curve.

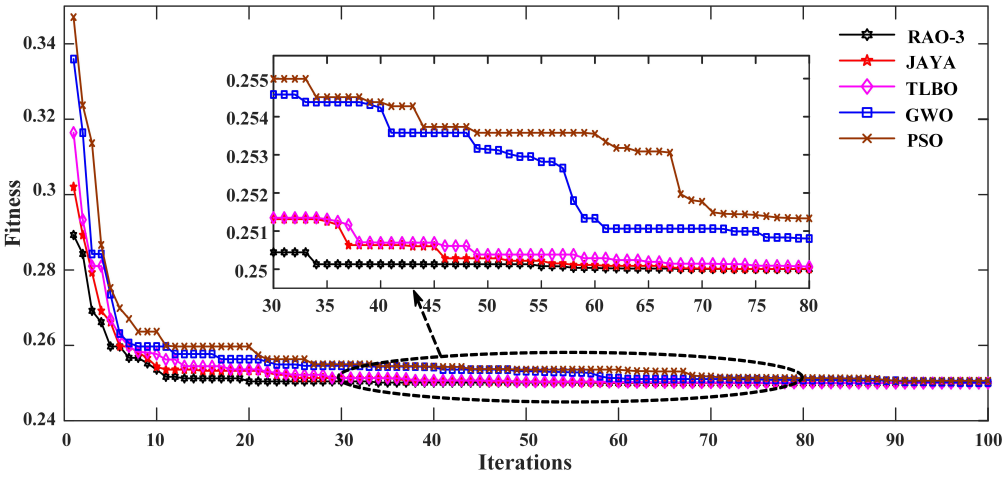

Figure 10. Fitness Curve of DG and DSTATCOM.

Table 5. Optimum number of EVs and optimum locations of EVCSs.

Fuzzy PSO		Fuzzy GWO		Fuzzy TLBO		Fuzzy JAYA		Fuzzy RAO-3	
Optimum node for EVCS	Optimum no of EV	Optimum node for EVCS	Optimum no of EV	Optimum node for EVCS	Optimum no of EV	Optimum node for EVCS	Optimum no of EV	Optimum node for EVCS	Optimum no of EV
60	35	6	40	30	41	18	37	30	36
42	37	40	35	18	43	39	37	60	33
20	35	10	36	7	33	42	49	6	44
6	41	45	40	40	33	33	36	40	40
30	37	19	34	61	36	24	36	18	45
Total no. of EV	185	Total no. of EV	185	Total no. of EV	186	Total no. of EV	195	Total no. of EV	198

Table 6. Performance of the 69-bus radial distribution system after installation of the EVCS.

Scenario 1	Base Case	Two-Stage Methodology [20]	Fuzzy PSO	Fuzzy GWO	Fuzzy TLBO	Fuzzy JAYA	Fuzzy RAO-3
Real Power loss (kW)	224.56	41.01	43.383	40.6822	40.4744	40.1027	34.4876
Voltage minimum (p.u.)	0.902	0.9659	0.9671	0.9678	0.9689	0.9698	0.97653

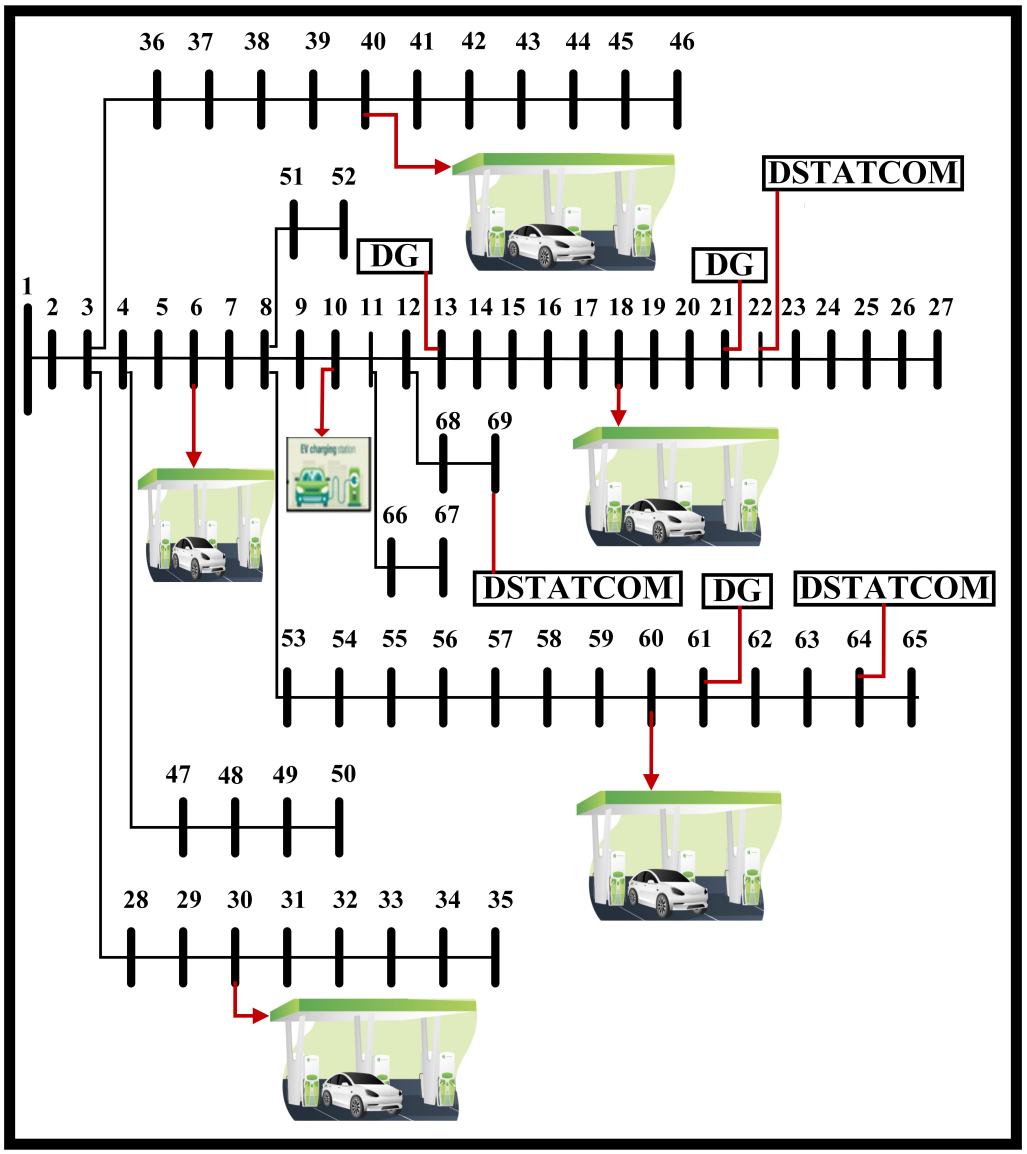

Figure 11. The single-line diagram of the 69-bus radial distribution system of scenario 1.

5.1.2. Scenario 2

In this work, DG, DSTATCOM, and EVCS were simultaneously (and optimally) placed via fuzzy multi-objective functions, as explained in Equation (15). In this scenario, the overall real power loss of the DST is reduced to 21.6085 kW, the voltage profile is enhanced, i.e., the minimum voltage of the DST is 0.988507 p.u. The optimum number of electric vehicles is increased, i.e., 209.

The optimum locations and sizings of DG and DSTATCOM were conducted, as shown in Tables 7 and 8. The optimal number of EVs and optimal locations of EVCSs were placed in the distribution system, as shown in Table 9. The performance of the distribution system can be analyzed in Table 10. The voltage profile curve and fitness function curves are shown in Figures 12 and 13. The single-line diagram of the 69-bus radial distribution system with EVCS, DG, and DSTATCOM of scenario 2 is shown in Figure 14.

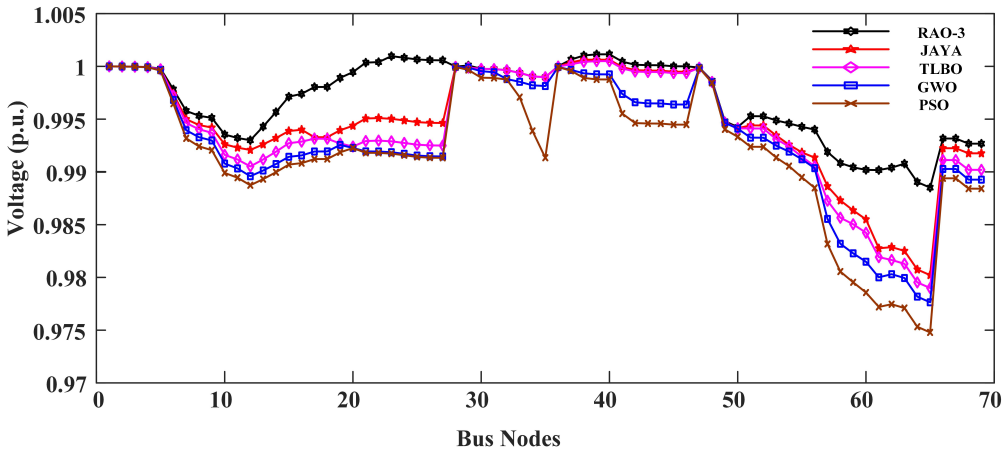

Figure 12. Voltage curve.

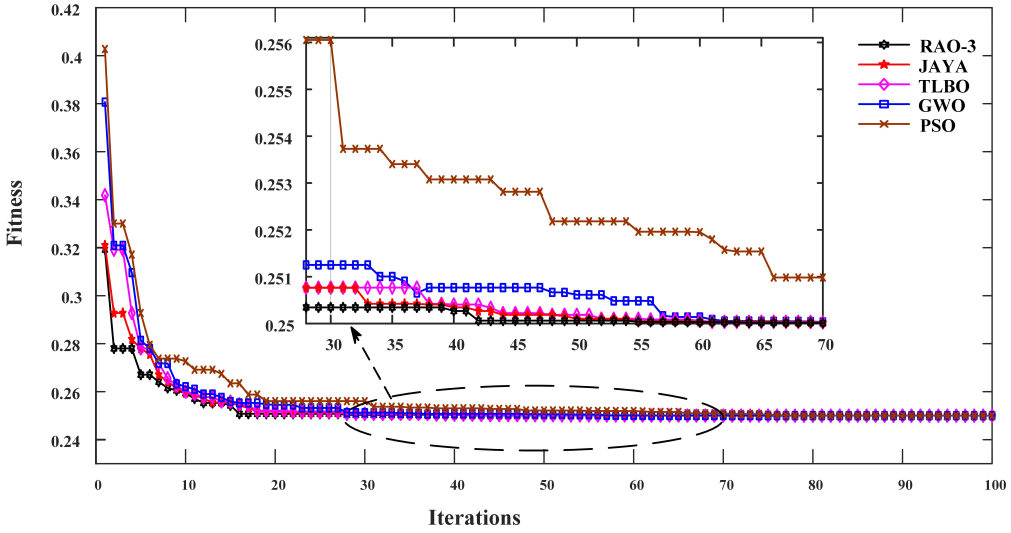

Figure 13. Fitness curve.

Table 7. DG optimum location and sizing.

Fuzzy PSO		Fuzzy GWO		Fuzzy TLBO		Fuzzy JAYA		Fuzzy RAO-3	
DG Node location	DG Sizing (kW)	DG Node location	DG Sizing (kW)	DG Node location	DG Sizing (kW)	DG Node location	DG Sizing (kW)	DG Node location	DG Sizing (kW)
21	653.8921	21	484.88	61	721.5755	14	489.8753	13	468.1426
61	780.7009	61	875.5393	13	482.7538	23	574.7970	61	900.0000
16	466.1071	12	540.2767	22	696.3707	61	836.0277	21	532.5574

Table 8. DSTATCOM optimum location and sizing.

Fuzzy PSO		Fuzzy GWO		Fuzzy TLBO		Fuzzy JAYA		Fuzzy RAO-3	
Node location	Sizing (kVAr)	Node location	Sizing (kVAr)	Node location	Sizing (kVAr)	Node location	Sizing (kVAr)	Node location	Sizing (kVAr)
69	361.1784	69	299.43	23	313.5098	68	462.5327	64	468.3387
21	488.7751	64	673.4	69	466.6435	64	673.4000	69	464.8292
64	506.5490	24	388.42	64	598.5872	22	239.8411	22	446.1719

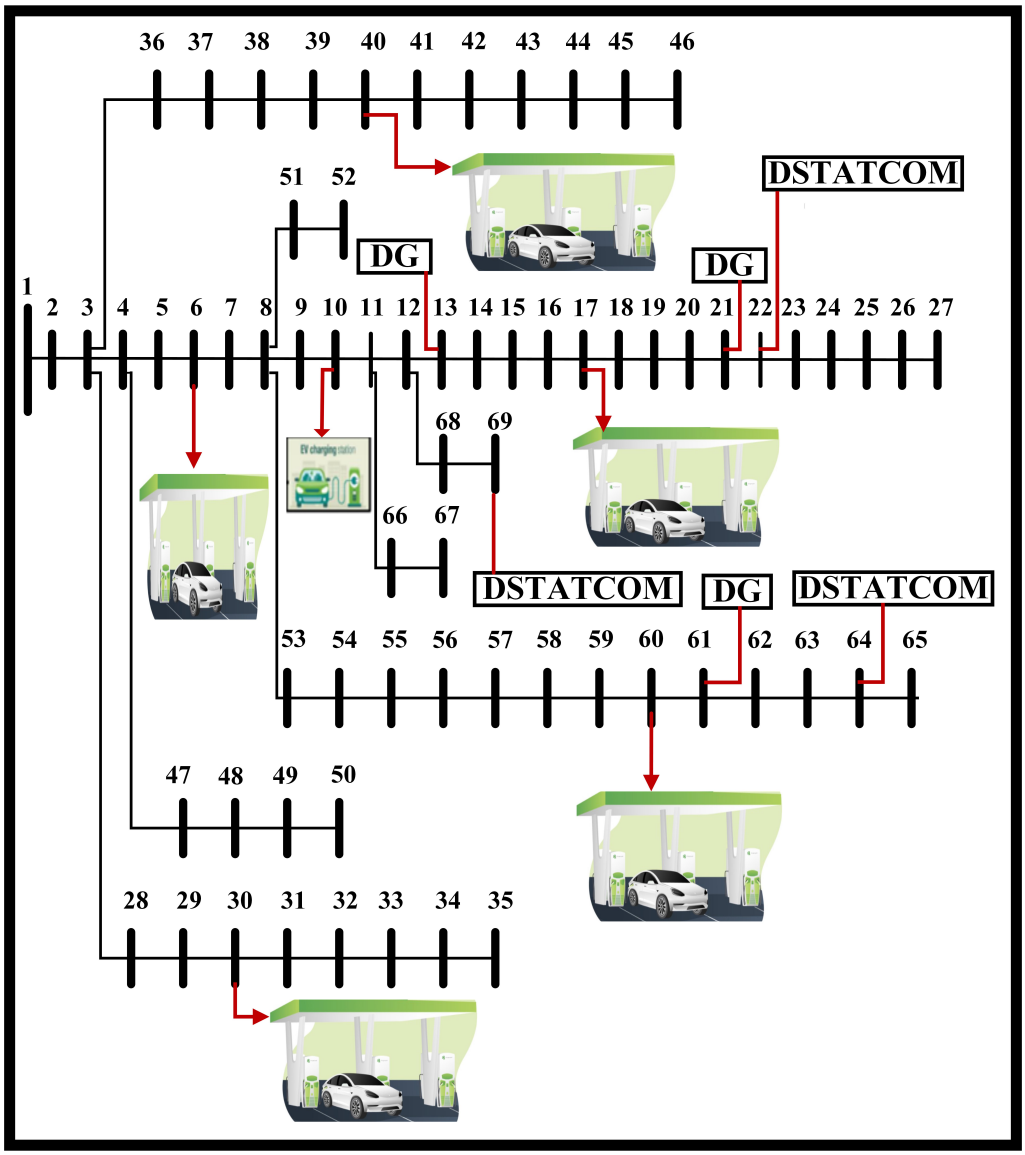

Figure 14. The single-line diagram of the 69-bus radial distribution system of scenario 2.

Table 9. Optimum number of EVs and optimum locations of EVCSs.

Fuzzy PSO		Fuzzy GWO		Fuzzy TLBO		Fuzzy JAYA		Fuzzy RAO-3	
Optimum node for EVCS	Optimum no of EV	Optimum node for EVCS	Optimum no of EV	Optimum node for EVCS	Optimum no of EV	Optimum node for EVCS	Optimum no of EV	Optimum node for EVCS	Optimum no of EV
39	41	59	30	39	44	59	39	40	47
30	39	30	41	31	36	5	48	60	40
4	33	41	39	18	37	41	40	17	36
17	28	18	33	6	38	18	35	30	40
60	45	6	43	60	35	60	37	5	46
Total no. of EV	186	Total no. of EV	186	Total no. of EV	190	Total no. of EV	199	Total no. of EV	209

Table 10. Performance comparison of the 69-bus system.

Scenario 2	Base Case	Fuzzy PSO	Fuzzy GWO	Fuzzy TLBO	Fuzzy JAYA	Fuzzy RAO-3
SS Real power (kW)	4027.19	2220.7	2203.8	2163.3	2156.8	2119.1
SS Reactive power (kVAr)	2796.77	729.6046	724.4771	711.0508	708.7443	706.7995
SS Power factor	0.8214	0.95 lag	0.95 lag	0.95 lag	0.95 lag	0.95 lag
DG Penetration (kW)	-	1900.7	1900.7	1900.6997	1900.7	1900.7
Active Power loss (kW)	224.56	26.5745	23.985	22.1920	22.1257	21.6085
Voltage minimum (p.u.)	0.902	0.974789	0.977643	0.978995	0.980217	0.988507

In scenario 2, the active power loss was reduced to 90.377%, 47.30%, and 37.341% compared to the base case, two-stage methodology [20], and scenario 1. The minimum voltage of the bus was enhanced to 0.988507 p.u. and 0.97653 p.u. in scenario 2 and scenario 1 compared to the base case minimum voltage of 0.902 p.u. The optimum number of vehicles in scenario 2 increased to 10% and 5.56% compared to the two-stage methodology [20] in scenario 1. Table 11 displays the comparison findings for all scenarios.

Table 11. Comparison results.

Cases	Real Power Loss (kW)	Voltage Minimum (p.u.)	Total Number of EV
Scenario 2	21.6085	0.988507	209
Scenario 1	34.4876	0.97653	198
Two-stage methodology [20]	41.01	0.9461	190
Base Case	224.56	0.9020	-

5.2. Analysis of the Enhancement of Distribution Load Growth

In this section, with the initial EV charging load with a simultaneous approach (scenario 2), the effect of enhancement of the distribution load is analyzed for the 69-bus radial DST in Figure 15. Active power loss decreases immensely with the integration of DSTATCOM and DGs in comparison to the base case. From Table 12, the real power loss reduces with the proposed methodology.

Table 12. The impact of the increased distribution load on the 69-bus.

Load Factor	Base-Case	Two Stage Methodology [20]	Fuzzy PSO	Fuzzy GWO	Fuzzy TLBO	Fuzzy JAYA	Fuzzy RAO-3
1	224.8949	41.01	26.5745	23.985	22.1920	22.1257	21.6085
1.1	277.3206	59.22	44.7845	42.195	40.402	40.3357	39.8185
1.2	336.5602	89.22	67.8	65.195	63.402	63.34	62.82
1.3	403.0962	110.27	95.8345	93.245	91.452	91.3857	90.8685
1.4	477.4605	143.65	129.1845	126.6	124.842	124.7357	124.22
1.5	560.2671	182.66	168.1945	165.605	163.812	163.75	163.2285

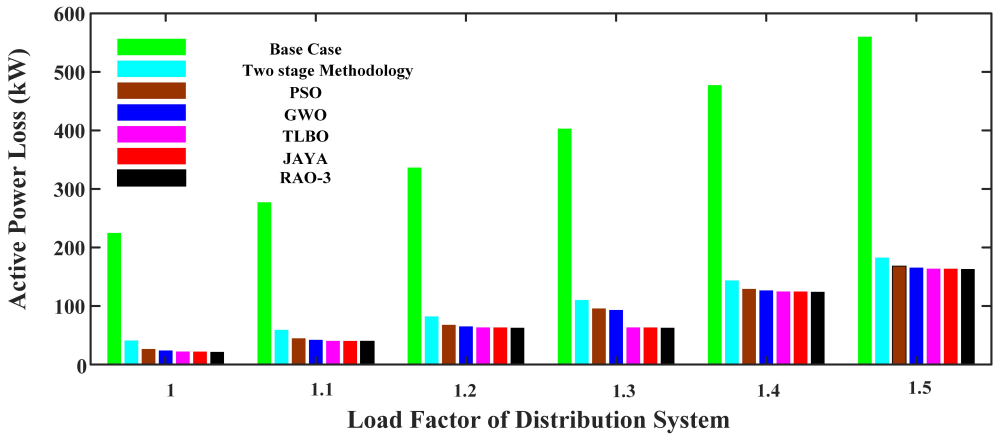

Figure 15. The impact of the rising DST system load on the performance of the 69-bus radial distribution system.

5.3. Analysis of Enhancement of EV Load

In this section, the effect of the enhancement of an EV load is analyzed with a simultaneous approach (scenario 2) with different load factors of the distribution system. The proposed method of scenario 2 has the best performance compared to other scenarios. The EV load is increased up to 50 % of the initial load. Due to the enhancement of the EV load at various load conditions in distribution systems shown in Table 13, the power loss rises with rises in the EV load; however, with the fuzzy RAO-3 simultaneously proposed approach, the power loss is compared less with the base case.

The impact of the active power and reactive power consumed from SS with the enhancement of the EV load is depicted in Tables 14 and 15. Active power and reactive power consumed from SS can meet the rise in the EV load; with a simultaneously proposed approach, both active and reactive power consumed is less than the base case.

When the EV load increases, the impact on the minimum bus node voltage is analyzed in Table 16. From Table 16, the minimum voltage reduces with a gradual enhancement of the EV load, and with a fuzzy RAO-3 simultaneous approach, a minimum bus node voltage remains within the standard limits.

Table 13. Impact on the active power loss (kW) in a 69-bus radial DST.

Load Factor	Base Case	Initial EV Load	With 25% Rise in EV Load	With 40% Rise in EV Load	With 50% Rise in EV Load
0.4	32.51	11.4535	13.652	18.943	20.5833
0.5	51.61	12.8789	15.0161	20.2530	21.2379
0.6	75.53	16.3617	18.2900	22.8646	23.5342
0.7	104.53	18.5627	20.7933	23.6172	26.2366
0.8	138.90	20.2054	22.0611	24.1741	28.5975
0.9	178.95	20.7181	23.432	25.5596	29.7692
1	225	21.6085	25.7404	26.8496	32.1375

Table 14. Impact on the active power (kW) consumed from SS in the 69-bus radial DST.

Load Factor	Base Case	Initial EV Load	With 25% Rise in EV Load	With 40% Rise in EV Load	With 50% Rise in EV Load
0.4	1553.39	1832.4	1954.38	2167.342	2239.6
0.5	1952.70	1928.1	2053.6	2207.3	2272.7
0.6	2356.84	1956.6	2155.5	2249.3	2316.2
0.7	2766.07	2015.1	2197	2283.1	2356.8
0.8	3180.66	2072.4	2200.8	2303.5	2379.9
0.9	3600.92	2104.3	2218.3	2331.0	2397.362
1	4027.19	2119.1	2247.8	2352.6	2405.1

Table 15. Impact on the reactive power (kVAr) consumed from SS in the 69-bus radial DST.

Load Factor	Base Case	Initial EV Load	With 25% Rise in EV Load	With 40% Rise in EV Load	With 50% Increase in EV Load
0.4	1092.69	601.2	631.21	710.95	731.8654
0.5	1370.85	630.1	678.551	725.066	745.5750
0.6	1651.20	641.3	700.4033	738.028	758.9
0.7	1933.83	652.53	723.6628	759.084	767.6204
0.8	2218.88	678.56	731.396	763.02	779.3336
0.9	2506.48	693.68	738.963	770.873	788.2645
1	2796.77	706.79	743.377	775.829	793.3322

Table 16. Impact on the minimum distribution bus node 69-bus radial DST.

Load Factor	Base Case	Initial EV Load	With 25% Rise in EV Load	With 40% Rise in EV Load	With 50% Rise in EV Load
0.4	0.9656	0.9970	0.9943	0.9858	0.9883
0.5	0.9574	0.9899	0.9861	0.9841	0.9824
0.6	0.9476	0.9893	0.9848	0.9833	0.9812
0.7	0.9383	0.9891	0.9837	0.9824	0.9780
0.8	0.9288	0.9889	0.9831	0.9792	0.9777
0.9	0.9191	0.9887	0.9825	0.9778	0.9768
1	0.9092	0.9885	0.9820	0.9714	0.9667

5.4. Analysis of Transient Responses

Figure 16 depicts the impacts of EVs on EVCS node voltages. Batteries charge from a fully depleted to a completely charged state for 69-bus radial distribution systems under peak load conditions. It is also worth noting that, even with EV charging demand, the voltage quality may be maintained at a deservedly high level due to the availability of the complete DG capacity and DSTATCOM installations.

In summary, the suggested approach enhances the test distribution system's performance, such as in scenario 2; compared to the base case active power loss reducing to 90.377%, the voltage profile is enhanced to 0.988507 p.u.

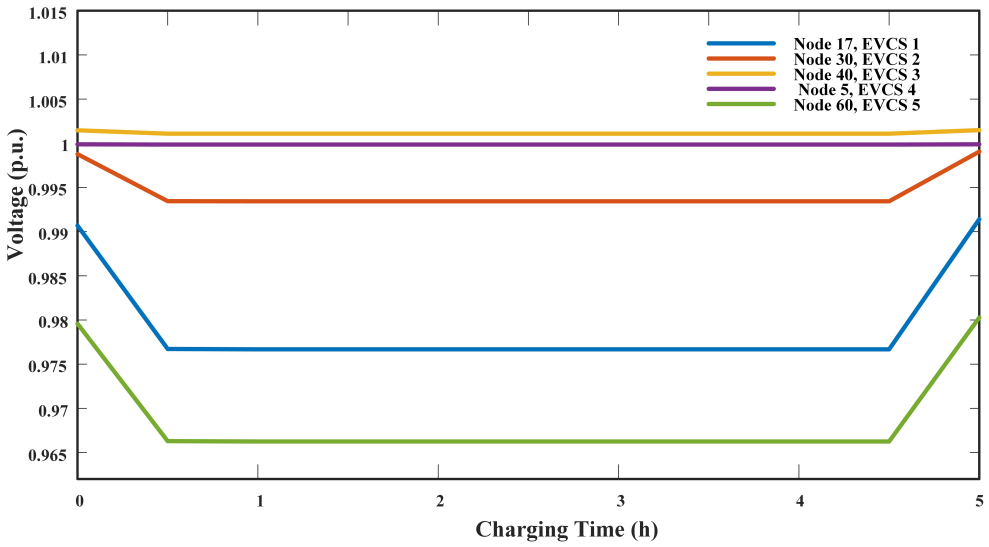

Figure 16. EVCS voltage transients.

6. Conclusions

This article proposes a simultaneous fuzzy approach for optimally planning electric vehicle charging stations, distributed generators, and shunt capacitors on 69-bus radial

distribution systems. In this work, two-stage placements and simultaneous placements of EVCS, DG, and DSTATCOM were performed using the RAO-3 algorithm. Li-ion characteristic curves were used to develop P and Q load models for EV battery charging. Simulation results show that SS can support an EV load up to its active power supply's maximum level after the impact of the EV load growth under various loading situations. With the help of DG and DSTATCOM, the voltage profile can be kept at a reasonable level despite an increase in the EV load. The node voltages at the EVCS are impacted by the transient battery charging load, and at steady state charging, the node voltage maintains fair values with the help of DG and DSTATCOM. We show that the proposed method outperforms the stage-wise placement of various components in terms of (1) reducing active power loss, (2) improving substation power factors, (3) enhancing distribution network voltage profiles, and (4) allocating the optimum number of vehicles at the charging stations. The present work can be extended to vehicle-to-grid technology.

Author Contributions: Conceptualization, A.K.M. and S.R.S.; methodology, A.K.M., P.S.B. and S.R.S.; software, A.K.M.; validation, A.K.M. and P.S.B.; review and editing, A.K.M., P.S.B. and S.R.S. All authors have read and agreed to the published version of the manuscript.

Funding: Woosong University's Academic Research Funding—2022.

Institutional Review Board Statement: Not applicable.

Informed Consent Statement: Not applicable.

Data Availability Statement: Not applicable.

Conflicts of Interest: The authors declare no conflict of interest.

Abbreviations

The following abbreviations are used in this manuscript:

EVs	Electrical Vehicles
EVCS	Electric Vehicle charging stations
NEV	Optimum number of electrical vehicles
DST	Distribution System
DG	Distributed Generators
DSTATCOM	Distribution Static Compensator
SS	Substation
pf	power factor
GWO	Grey Wolf Optimizer
PSO	Particle Swarm Optimization
TLBO	Teaching-Learning-Based Optimization
$RPLX$	Real power loss index
RPL_{DGSC}	Active power loss with DG and DSTATCOM
RPL_{Base}	Real power loss with base case
P^{DG}	Capacity of DG
ndg	Number of DG
P_j^{load}	Active power load connected at jth bus
nb	Total number of buses in the distribution network
Pl	Active power loss of the distribution network when DG or DSTATCOM or EV charging stations are installed
Ql	Reactive power loss of the distribution network when DG or DSTATCOM are installed
$EVPI^{EVLD}$	Active power loss with EV and other load losses
$EVPI^{LD}$	Load losses
F_{zdc}	Multi-objective fuzzy functions for optimum location and sizing of DG and DSTATCOM
F_{ze}	Fuzzy objective functions for optimum location and sizing of EVCS
F_{zs}	Multi-objective fuzzy functions for simultaneous optimum location and sizing of EV, DG, and DSTATCOM

P_k^{DG}	DG power injection at the nodes in the distribution network
Q_m^{sc}	DSTATCOM reactive power injection at the nodes in the distribution network
$itrmax$	Maximum iteration
itr	Present iteration

References

1. Al-Thani, H.; Koç, M.; Isaifan, R.J.; Bicer, Y. A Review of the Integrated Renewable Energy Systems for Sustainable Urban Mobility. *Sustainability* **2022**, *14*, 10517. [CrossRef]
2. Kalakanti, A.K.; Rao, S. Charging Station Planning for Electric Vehicles. *Systems* **2022**, *10*, 6. [CrossRef]
3. Ali, A.; Shakoor, R.; Raheem, A.; Muqeet, H.A.U.; Awais, Q.; Khan, A.A.; Jamil, M. Latest Energy Storage Trends in Multi-Energy Standalone Electric Vehicle Charging Stations: A Comprehensive study. *Energies* **2022**, *15*, 4727. [CrossRef]
4. Ahmad, F.; Iqbal, A.; Ashraf, I.; Marzb, M. Optimal location of electric vehicle charging station and its impact on distribution network: A review. *Energy Rep.* **2022**, *8*, 2314–2333. [CrossRef]
5. Moghaddam, Z.; Ahmad, I.; Habibi, D.; Phung, Q.V. Smart Charging Strategy for Electric Vehicle Charging Stations. *IEEE Trans. Transport. Electrif.* **2018**, *4*, 76–88. [CrossRef]
6. Awasthi, A.; Venkitusamy, K.; Padmanaban, S.; Selvamuthukumaran, R.; Blaabjerg, F.; Singh, A.K. Optimal planning of electric vehicle charging station at the distribution system using hybrid optimization algorithm. *Energy* **2017**, *133*, 70–78. [CrossRef]
7. Kongjeen, Y.; Bhumkittipich, K.; Mithulananthan, N.; Amiri, I.S.; Yupapin, P. A modified backward and forward sweep method for microgrid load flow analysis under different electric vehicle load mathematical models. *Electr. Power Syst. Res.* **2019**, *168*, 46–54. [CrossRef]
8. Yang, X.; Zhang, Y. A comprehensive review on electric vehicles integrated in virtual power plants. *Sustain. Energy Technol. Assess.* **2021**, *48*, 101678. [CrossRef]
9. Aljehane, N.O.; Mansour, R.F. Optimal allocation of renewable energy source and charging station for PHEVs. *Sustain. Energy Technol. Assess.* **2021**, *49*, 101669. [CrossRef]
10. Mohanty, A.K.; Suresh, B.P. Multi-objective Optimal Planning of Fast Charging station and Distributed Generators in a Distribution Systems. In Proceedings of the IEEE 2nd International Conference on Electrical Power and Energy Systems (ICEPES), Bhopal, India, 10–11 December 2021; pp. 1–6. [CrossRef]
11. Roudbari, A.; Nateghi, A.; Yousefi-khanghah, B.; Asgharpour-Alamdari, H.; Zare, H. Resilience-oriented operation of smart grids by rescheduling of energy resources and electric vehicles management during extreme weather condition. *Sustain. Energy Technol. Assess.* **2021**, *28*, 100547. [CrossRef]
12. Piazza, G.; Bracco, S.; Delfino, F.; Siri, S. Optimal design of electric mobility services for a Local Energy Community. *Sustain. Energy Technol. Assess.* **2021**, *26*, 100440. [CrossRef]
13. Palmiotto, F.; Zhou, Y.; Forte, G.; Dicorato, M.; Trovato, M.; Cipcigan, L.M. A coordinated optimal programming scheme for an electric vehicle fleet in the residential sector. *Sustain. Energy Grids Netw.* **2021**, *28*, 100550. [CrossRef]
14. Dekaraja, B.; Saikia, L.C. Impact of electric vehicles and realistic dish-Stirling solar thermal system on combined voltage and frequency regulation of multiarea hydrothermal system. *Energy Storage* **2022**, e370 . [CrossRef]
15. Ahmad, F.; Khalid, M.; Panigrahi, B.K. An enhanced approach to optimally place the solar powered electric vehicle charging station in distribution network. *J. Energy Storage* **2021**, *42*, 103090. [CrossRef]
16. Liu, L.; Zhang, Y.; Da C.; Huang, Z.; Wang, M. Optimal allocation of distributed generation and electric vehicle charging stations based on intelligent algorithm and bi-level programming. *Int. Trans. Electr. Energy Syst.* **2020**, *30*, e12366. [CrossRef]
17. Dharavat, N.; Sudabattula, S.K.; Velamuri, S.; Mishra, S.; Sharma, N.K.; Bajaj, M.; Elgamli, E.; Shouran, M.; Kamel, S. Optimal allocation of renewable distributed generators and electric vehicles in a distribution system using the political optimization algorithm. *Energies* **2022**, *15*, 6698. [CrossRef]
18. Biswas, P.P.; Mallipeddi, R.; Suganthan, P.N.; Amaratunga, G.A. A multiobjective approach for optimal placement and sizing of distributed generators and capacitors in distribution network. *Appl. Soft Comput.* **2017**, *60*, 268–280. [CrossRef]
19. Bilal, M.; Rizwan, M. Integration of electric vehicle charging stations and capacitors in distribution systems with vehicle-to-grid facility. *Energy Sources Part A Recover. Util. Environ. Effects* **2021**, 1–30. [CrossRef]
20. Gampa, S.R.; Jasthi, K.; Goli, P.; Das, D.; Bansal, R.C. Grasshopper optimization algorithm based two stage fuzzy multiobjective approach for optimum sizing and placement of distributed generations, shunt capacitors and electric vehicle charging stations. *J. Energy Storage* **2020**, *27*, 101117. [CrossRef]
21. Sirjani, R.; Jordehi, A.R. Optimal placement and sizing of distribution static compensator (D-STATCOM) in electric distribution networks: A review. *Renew. Sustain. Energy Rev.* **2017**, *77*, 688–694. [CrossRef]
22. Jazebi, S.; Hosseinian, S.H.; Vahidi, B. DSTATCOM allocation in distribution networks considering reconfiguration using differential evolution algorithm. *Energy Convers. Manag.* **2011**, *52*, 2777–2783. [CrossRef]
23. Devi, S.; Geethanjali, M. Optimal location and sizing determination of Distributed Generation and DSTATCOM using Particle Swarm Optimization algorithm. *Int. J. Electr. Power Energy Syst.* **2014**, *62*, 562–570. [CrossRef]
24. Salkuti, S.R. Optimal allocation of DG and D-STATCOM in a distribution system using evolutionary based Bat algorithm. *Int. J. Adv. Comput. Sci. Appl.* **2021**, *12*, 802–810. [CrossRef]

25. Yuvaraj, T.; Ravi, K.; Devabalaji, K.R. DSTATCOM allocation in distribution networks considering load variations using bat algorithm. *Ain Shams Eng. J.* **2017**, *8*, 391–403. [CrossRef]
26. Pratap, A.; Tiwari, P.; Maurya, R.; Singh, B. Minimisation of electric vehicle charging stations impact on radial distribution networks by optimal allocation of DSTATCOM and DG using African vulture optimization algorithm. *Int. J. of Ambient Energy* **2022**, 1–20. [CrossRef]
27. Safari, A.; Babaei, F.; Farrokhifar, M. A load frequency control using a PSO-based ANN for micro-grids in the presence of electric vehicles. *Int. J. Ambient. Energy* **2021**, *42*, 688–700. [CrossRef]
28. Singh, J.; Tiwari, R. Real power loss minimisation of smart grid with electric vehicles using distribution feeder reconfiguration. *IET Gener. Transm. Distrib.* **2019**, *13*, 4249–4261. [CrossRef]
29. Babu, P.V.; Swarnasri, K. Multi-objective optimal allocation of electric vehicle charging stations in radial distribution system using teaching learning based optimization. *Int. J. Renew. Energy Res.* **2020**, *10*, 366–377.
30. Mohanty, A.K.; Babu, P.S. Optimal placement of electric vehicle charging stations using JAYA algorithm. In *Recent Advances in Power Systems*; Springer: Singapore, 2021; pp. 259–266.
31. Rao, R. Rao algorithms: Three metaphor-less simple algorithms for solving optimization problems. *Int. J. Ind. Eng. Comput.* **2020**, *11*, 107–130. [CrossRef]
32. Qian, K.; Zhou, C.; Allan, M.; Yuan, Y. Modeling of load demand due to EV battery charging in distribution systems. *IEEE Trans. Power Syst.* **2010**, *26*, 802–810. [CrossRef]
33. Masoum, A.S.; Deilami, S.; Moses, P.S.; Abu-Siada, A. Impacts of battery charging rates of plug-in electric vehicle on smart grid distribution systems. In Proceedings of the IEEE PES Innovative Smart Grid Technologies Conference Europe (ISGT Europe), Gothenburg, Sweden, 11–13 October 2010; pp. 1–6.
34. Khalid, M.; Ahmad, F.; Panigrahi, B.K.; Al-Fagih, L. A comprehensive review on advanced charging topologies and methodologies for electric vehicle battery. *J. Energy Storage* **2022**, *53*, 105084. [CrossRef]
35. Asker, Z.L.; Klir, G.J.; Yuan, B. *Fuzzy Sets, Fuzzy Logic, and Fuzzy Systems: Selected Papers*; World Scientific: Singapore, 1996; Volume 6.
36. Savier, J.S.; Das, D. Impact of network reconfiguration on loss allocation of radial distribution systems. *IEEE Trans. Power Deliv.* **2007**, *22*, 2473–2480. [CrossRef]